Applied Petrochemical Research (2018) 8:153–162
https://doi.org/10.1007/s13203-018-0203-z

ORIGINAL ARTICLE

Hydrogenation of levulinic acid with and without external hydrogen over Ni/SBA-15 catalyst

Mohan Varkolu[1] · Hari Babu Bathula[2,3] · Young-Woong Suh[2,3] · David Raju Burri[1] · Seetha Rama Rao Kamaraju[1]

Received: 10 January 2017 / Accepted: 4 June 2018 / Published online: 14 June 2018

Abstract
A series of Ni/SBA-15 catalysts were prepared by impregnation method for the hydrogenation of levulinic acid (LA) to γ-valerolactone in a fixed bed reactor at atmospheric pressure. The catalysts were characterized by XRD, TPR, AAS, Pulse chemisorption, SEM-EDAX, TEM, BET Surface area and XPS. The catalyst 30 wt% Ni/SBA-15 exhibited excellent catalytic performance (97% yield) at 250 °C due to the presence of superior number of active surface Ni species. While 30 wt% Ni/SiO_2 catalyst showed lower catalytic activity (87% yield) at about similar conversion. The co-feeding of formic acid (FA) and water (impurities) with levulinic acid was also evaluated over 30 wt% Ni/SBA-15 which yielded excellent levulinic acid conversion. The noteworthy results were obtained at a molar ratio of FA/LA = 5. The constant catalytic activity during 10 h experiment with an external H_2 flow has showed the sturdiness of the Ni/SBA-15 catalyst. On the other hand, a slight decrease in conversion as well as yield during the time-on-stream in the absence of external H_2 flow was attributed to the accumulation of carbon species on the catalyst surface.

Keywords Hydrogenation · Levulinic acid · γ-Valerolactone · With external H_2 · Without external H_2 · 30 wt% Ni/SBA-15

Introduction

The adverse climate change symptoms need immediate alleviation measures. Excessive exploitation of non-renewable sources of energy and environment unfriendly practices (fossil fuels) need to be curtailed to address the issues of energy security nationally and globally. Though several renewable sources exist, the fourth most abundant renewable source is the biomass after coal, natural gas, and crude oil. Biomass is perennial and its utilization will be beneficial for the environmental concerns. Biomass is a practically inexhaustible renewable source that can potentially facilitate the transition from the exhaustible fossil fuels and, currently, biomass is providing 14% of energy to the society globally.

Statistically, India produces about 450–500 million tonnes of biomass per annum. Amongst, around 120–150 million metric tonnes per annum is obtained from forestry and agriculture waste. At present, biomass is providing 32% of all the primary energy utilizing in the country [1]. In this regard, Energy Alternatives India (EAI) estimate that the potential in the short-term for power generation from biomass in India varies from about 18,000 MW, when the scope of biomass is as traditionally defined, to a high of about 50,000 MW if one would be able to expand the scope of definition of biomass [1]. Currently, 5% blending of ethanol in gasoline (biofuel) taking place as per the government decision which is subtle in entire fuel consumption. India targets the usage of 20% of biofuels by the year 2020. In this aspect, utilization of biomass and/or biomass-derived derivatives is promising not only due to the dwindling of fossil fuels but also the stringent regulations on the composition and quality of the transportation fuels. Among the biomass-derived chemicals, levulinic acid (LA) is an important candidate that has been classified by top 12 promising attractive chemicals [2, 3] and it can be accessible through acid hydrolysis of cellulose [4], and also as a by-product in a paper industry [5].

✉ Mohan Varkolu
mohan.iict@gmail.com

✉ Seetha Rama Rao Kamaraju
ksramarao@iict.res.in

[1] Inorganic and Physical Chemistry Division, CSIR-Indian Institute of Chemical Technology, Hyderabad, India 5000071

[2] Department of Chemical Engineering, Hanyang University, Seoul 133-691, Republic of Korea

[3] Research Institute of Industrial Science, Hanyang University, Seoul 133-691, Republic of Korea

Moreover, LA is considered as an important intermediate for the production of the plethora of commodity products by different methods, viz., oxidation [6], reduction [7], condensation [8], reductive amination [9, 10] and esterification [11, 12]. The reduction gave the plethora of useful chemicals, fuels and fuel additives. Accordingly, reduction of LA can be accomplished by two different methods such as formic acid as a sole hydrogen source [13–17] or H_2 as an external hydrogen source [18–28] with either homogeneous [29–31] or heterogeneous catalysts [20–24, 26–28] at high pressures in the presence of solvents under batch or continuous process [32] conditions (Scheme1).

Despite the use of solvents and high pressures, the recovery of the catalyst is still a challenging task. However, only two reports were cited in the literature for the vapour phase hydrogenation of levulinic acid using noble metals and non-noble metal as catalysts by using 1, 4-dioxane as an additive [32, 33].

To make use of avoiding the separation of solvent from the product and un-reacted reactant, new and innovative approaches are needed for the green production of fuel. In this connection, the LA hydrogenation was performed under vapour phase conditions without using any additives at atmospheric pressure to produce γ-valerolactone [34]. γ-Valerolactone has a lot of applications as fuels and fuel additives [35–39]. These fuels have an advantage of low net emissions of global warming gas, CO_2. Even that low emissions is naturally recycled (further utilized by plant kingdom for photosynthesis) to produce biomass.

Besides, the catalytic systems have disadvantages like deactivation during the time-on-stream [34]. In order to enhance the stability and the selectivity of γ-valerolactone, we have chosen the mesoporous silica (SBA-15) as a support for supported Ni catalysts. The SBA-15 has wider pores, which enable better diffusion and transport of large reactant molecules [40]. Furthermore, Ni-based catalysts were reported for the dehydrogenation of formic acid [41] and formic acid can be used as a hydrogen source for the hydrogenation reactions [42]. Besides, formic acid can also perform hydrogenation reaction as a sole hydrogen source [43]. This concept encourages us to work with levulinic acid hydrogenation using formic acid as a hydrogen source. Additionally, we also observed prominent results with or without external hydrogen as the source.

Though the SiO_2-based supports were reported for the hydrogenation reactions. Among the SiO_2-based supports, ordered mesoporous silica materials such as SBA-15 are unique, owing to their remarkable properties such as high surface area (> 700 m^2/g), thermal stability, and uniform pore size (46–300 Å). This high surface area and uniform pore size of SBA-15 facilitate the high dispersion of active component even at higher loadings by retaining the mesoporous structure of SBA-15 [44–47]. Mesoporous materials have found potential applications in catalysis, as adsorbents, separation, optoelectronics, sensors, as supports, fabrication of nanostructure materials and so on.

In continuation to our ongoing research towards the development of Ni-based catalysts for the hydrogenation of biomass-derived platform molecules such as levulinic acid with or without external H_2 source (formic acid as a H_2 source), a series of Ni/SBA-15 catalysts were examined for this reaction. The present investigation highlights the application of mesoporous SBA-15 as an excellent support for enhancing the selectivity of γ-valerolactone over Ni/SBA-15 catalysts. Furthermore, this catalytic system is efficient for the production of γ-valerolactone with molecular H_2 and without external H_2 source (formic acid as a H_2 source).

Experimental

Synthesis of Ni supported SBA-15 catalysts

Mesoporous silica (SBA-15) was prepared by a self-assembly method using long chain surfactantP123 as template and tetraethylorthosilicate (TEOS) as SiO_2 source as reported by Zhao et al. [47]. Ni/SBA-15 catalysts with various loadings of Ni were prepared by wet impregnation method with an aqueous solution containing requisite amount of $Ni(NO_3)_2.6H_2O$ (AR grade obtained from M/s. Loba Chemie, India) and SBA-15 support. The prepared catalysts were dried overnight at 100 °C and calcined at 450 °C for 5 h.

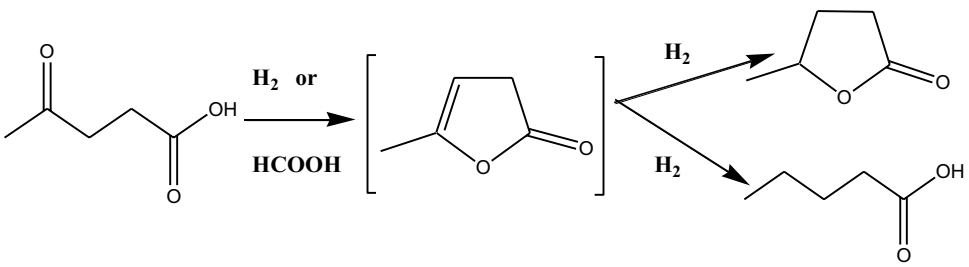

Scheme 1 Schematic representation of hydrogenation of levulinic acid to γ-valerolactone

Catalyst characterization

XRD patterns of the catalysts were recorded on a Rigaku Ultima-IV (M/s Rigaku Corporation, Japan) X-ray diffractometer having Ni-filtered Cu Kα radiation ($\lambda = 1.5406$ Å) with a scan speed of 4° min^{-1} and a scan range of 2°–80° at 40 kV and 20 mA.

The mesoporous nature of the SBA-15 is presented in a scan range of 0.7°–5°. Surface area, pore size and pore volume of all the catalysts were determined by N_2 adsorption–desorption isotherms at liquid N_2 temperature, i.e., 77 K (ASAP 2020 Adsorption unit, M/s. Micromeritics, USA). Brunauer, Emmett and Teller (BET) equation is used to calculate the surface area where as Barret–Joyner–Halenda (BJH) method is used to obtain the pore size distribution of the catalysts [48]. Prior to adsorption–desorption isotherms, the catalyst was degassed under vacuum at 250 °C for 1 h to remove the physisorbed moisture.

Temperature programmed reduction (TPR) of the catalysts was performed on AMI-90 TPR unit (M/s. Altamira Instruments, USA). About 50 mg of catalyst was placed in a quartz reactor and pre-treated in Ar flow 100 °C for 2 h. A flow of 5% H_2–Ar mixture gas (60 cm^3 min^{-1}) with a temperature ramping of 10 K min^{-1} was maintained. The hydrogen consumption was monitored using a thermal conductivity detector (TCD).

Ni content of catalysts was studied by atomic absorption spectroscope, AAS A-300 (M/s. Perkin–Elmer, Germany). The samples were prepared by dissolving in aqua regia.

The morphological features of the catalysts were obtained using a JEOL JEM 2000EXII transmission electron microscope, operating at 160 and 180 kV. The specimens were prepared by dispersing the samples in acetone using an ultrasonic bath and evaporating a drop of resultant suspension onto the lacey carbon support grid.

H_2 chemisorption using pulse (100 µL) titration procedure was carried out at 40 °C on an AUTOSORB-iQ, automated gas sorption analyser (M/s. Quantachrome Instruments, USA) to know the dispersion, metal particle size, and metal surface area of the catalysts. Prior to the experiment, the catalysts were reduced at 500 °C for 2 h followed by evacuation for 2 h.

Surface coverage (θ) was calculated by:

$$\theta = \text{AMSA}\ (\text{m}^2/\text{g}) \times 10^2 / S_{\text{BET}}\ (\text{m}^2/\text{g}),$$

where AMSA was active metal surface area.

Scanning electron microscope analysis was performed using (M/s. A LEO 1450) to obtain SEM image of the Ni/SBA-15 catalysts. Prior to the measurement, the samples were coated with gold by means of a Polaron SC sputter coater. The XPS analysis was carried out using an AXIS 165 apparatus (M/s. Kratos Instruments, UK) equipped with a dual anode (Mg and Al) using an Mg Kα source. The non-monochromatized Al Kα X-ray source ($h\upsilon = 1486.6$ eV) was operated at 12.5 kV and 16 mA. Analysis was done at room temperature and, before analysis, the samples were maintained under rigorous vacuum typically in the order of 10^{-8} Pa to avoid the accumulation of contaminants.

Activity test

With H_2 About 1 g of catalyst was sandwiched between the quartz wool in a fixed bed reactor made up of glass (300 mm long and 14 mm i.d.). Above the catalyst bed, silicon beads were placed which act as a preheating zone and ensures the reactant to get vaporizing before reaching the catalyst bed. The reactions were carried out in the temperature range of 250–295 °C with a liquid feed rate of 1 cm^3 h^{-1}. Prior to the reaction, the catalyst was reduced for 4 h at 500 °C in H_2 flow (30 cm^3 min^{-1}). Hydrogen gas flow rate of 1800 cm^3 h^{-1} was maintained during the course of the reaction while the nitrogen gas flow rate of 1800 cm^3 h^{-1} was maintained whenever the reaction performed without external H_2. The product mixture was collected at a regular intervals in an ice cooled trap and analyzed by a gas chromatograph equipped with Flame Ionization Detector (FID), GC-17A (M/s. Shimadzu Instruments, Japan) with OV-1 capillary column (30 m length, 0.53 mm id) and all the products were confirmed by GC–MS, QP 5050A (M/s. Shimadzu Instruments, Japan).

Without H_2 (i.e., formic acid as a H_2 source) Catalytic tests were carried out at atmospheric pressure in a glass down flow fixed bed reactor (300 mm long and 14 mm i.d.) loaded with 1 g of catalyst mixed with 1 g of quartz beads. Prior to the catalytic performance, the catalysts were reduced online at 500 °C for 4 h in H_2 flow (30 cm^3 min^{-1}). The feed solution consisting of requisite molar ratio of levulinic acid and formic acid was fed at a flow rate of 1 cm^3 min^{-1} through the micro perfusor feed pump in a stream of N_2 flow (30 cm^3 min^{-1}). The product mixture was collected at an outlet of the reactor and analyzed by a gas chromatograph equipped with a flame-ionization detector.

Results and discussion

The low angle X-ray diffraction patterns of Ni supported SBA-15 along with support SBA-15 are shown in Fig. 1. Three well-resolved diffraction peaks, one with a very intense peak at $2\theta = 0.9$–$1.18°$ and other two low intense peaks at $2\theta = 1.4$ and 1.8°, were shown by all the samples. These peaks were indexed to the (100), (110) and (200) planes which correspond to mesoporous structure of SBA-15 with hexagonal space group symmetry p6 mm [49, 50]. It is interesting to see the intactness of mesoporous structure

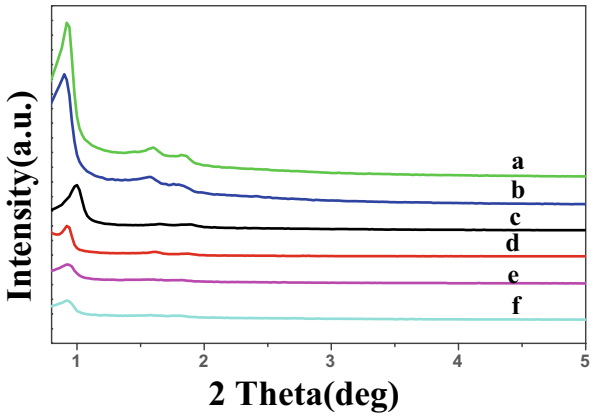

Fig. 1 SAXS patterns of **a** SBA-15, **b** 5Ni/SBA-15, **c** 10Ni/SBA-15, **d** 20Ni/SBA-15, **e** 30Ni/SBA-15, **f** 40Ni/SBA-15

of SBA-15 even after the deposition of higher Ni content (40 wt%). It was reported that the deposition of Ni (10 wt%) on SBA-15 support by liquid phase reductive deposition method did not alter the mesoporous structure of SBA-15 [44]. Similar observation was reported for Ru/SBA-15 catalysts [45]. In addition, intactness of SBA-15 structure was also reported for Ni/SBA-15 catalysts [46]. The present results are similar to the literature [44–46]. The decrease noticed in the intensity of (100), (110) and (200) diffraction peaks with the Ni content can be attributed to the reduced degree of ordering of mesoporous structure due to the presence of large quantity of NiO.

The wide-angle XRD patterns of the reduced Ni/SBA-15 catalysts are displayed in Fig. 2. Sharp diffraction peaks due to metallic Ni at 2θ values 44.5° (111), 53.0° (200) and 78.3° (220) (ICDD. No. 88-2326) can be seen in all catalysts. The broad peak at a 2θ value of ~22° is caused due to the amorphous nature of silica [51]. A very low intense NiO peak can also be seen at a 2θ value of ~40° in all catalysts.

N_2 adsorption–desorption isotherms of SBA-15 and Ni/SBA-15 catalysts are shown in Fig. 3. Figure 3 indicates that all the catalysts displayed a type IV isotherm with H1 hysteresis loop which is a characteristic of mesoporous material with uniform porosity as defined by IUPAC classification. A sharp inflection in P/P_0 range from 0.6 to 0.8 was found in the isotherms of SBA-15 and Ni/SBA-15 catalysts, providing the further proof of maintaining the mesoporous structure in the SBA-15 as well as even after the deposition of Ni on SBA-15 [52–54]. The isotherms of Ni/SBA-15 catalysts were very similar to that of SBA-15 support, but there was a slight variation in their inflation points as well as the N_2 adsorption amount. This clearly demonstrates that some modifications occurred in the channels of SBA-15 due to the presence of large quantity of NiO. The decrease in BET surface area (S_{BET}) upon deposition of Ni (Table 1) revealed that most of the active component was accumulated in the pores causing pore blockage. The unimodel pore volume distribution patterns of SBA-15 and Ni/SBA-15 are shown in Fig. 4. The pore diameter in the range of 50–90 Å in Ni/SBA-15 catalysts (Fig. 4) clearly designates the presence of uniform mesopores. The structural orderedness of SBA-15 remains intact even after the deposition of Ni. These results are in good agreement with the SAXS patterns. The pore size (Dp) of SBA-15 has been slightly enhanced by the deposition of Ni, which in turn decreases the pore wall thickness. The pore wall thickness (t) is in the range of 2–4 nm which is in accordance with the reported results [50, 54]. The Ni content determined by AAS is very close to those of theoretical values up to 30 wt% Ni. Beyond 30 wt% Ni loading, the values derived from AAS are lower compared to the theoretical values.

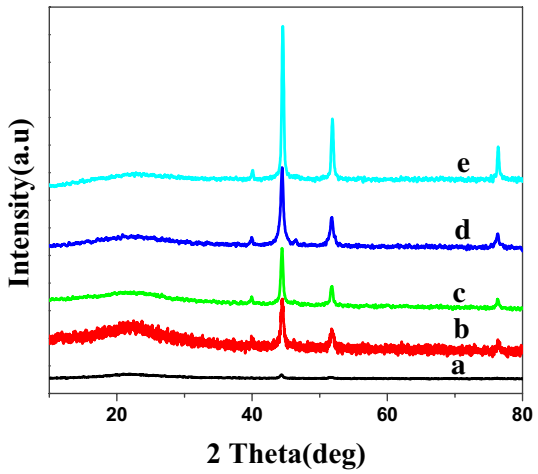

Fig. 2 Reduced XRD patterns of **a** 5Ni/SBA-15, **b** 10Ni/SBA-15, **c** 20Ni/SBA-15, **d** 30Ni/SBA-15, **e** 40Ni/SBA-15

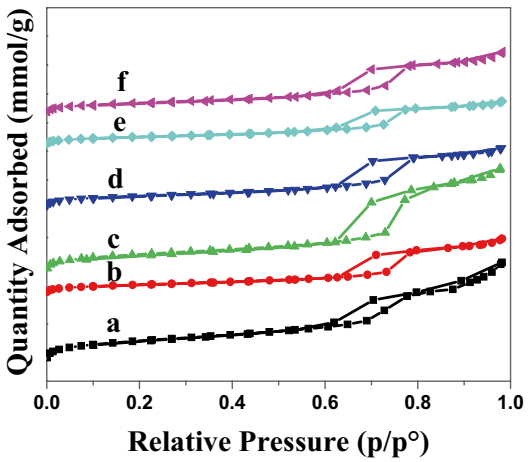

Fig. 3 N_2 adsorption–desorption isotherms of **a** SBA-15, **b** 5Ni/SBA-15, **c** 10Ni/SBA-15, **d** 20Ni/SBA-15, **e** 30Ni/SBA-15, **f** 40Ni/SBA-15

Table 1 Ni content, surface area, pore size distribution and XRD parameters of SBA-15 and Ni/SBA-15 catalysts

Catalyst	Ni content[a] (wt%)	S_{BET} ($m^2\ g^{-1}$)	Vp ($cm^3\ g^{-1}$)	Dp (nm)	$D^b_{(100)}$ (nm)	A^c_0 (nm)	Pore wall thickness ($t = a_0 - Dp$) nm
SBA-15	–	741	1.11	6.9	9.1	10.9	4.0
5Ni/SBA-15	5.0	596	1.19	8.7	9.8	11.4	2.7
10Ni/SBA-15	10.0	371	0.68	8.0	8.9	10.3	2.3
20Ni/SBA-15	20.0	367	0.72	8.5	9.6	11.1	2.6
30Ni/SBA-15	27.9	310	0.64	8.9	9.7	11. 2	2.3
40Ni/SBA-15	32.0	277	0.51	8.0	9.4	10.9	2.9

[a]Obtained from AAS

[b]Obtained from the (100) plane in the low angle XRD patterns

[c]$a_0 = 2d_{100} \times \sqrt{3}$

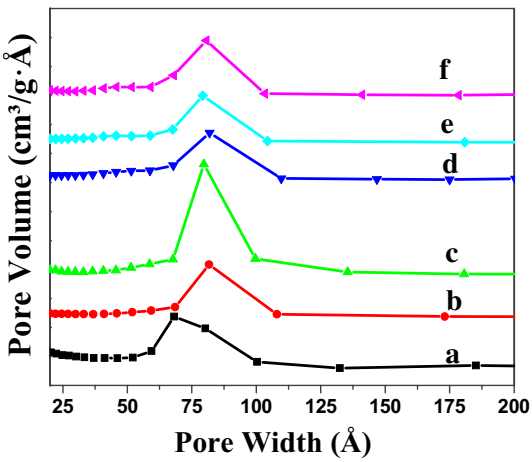

Fig. 4 Pore volume distribution patterns of **a** SBA-15, **b** 5Ni/SBA-15, **c** 10Ni/SBA-15, **d** 20Ni/SBA-15, **e** 30Ni/SBA-15, **f** 40Ni/SBA-15

H_2 chemisorption results are shown in Table 2. Based on the assumption that each Ni atom chemisorbs one H-atom, Ni dispersion (D %), Ni-metal surface area (AMSA) and Ni particle sizes were determined. The number of surface Ni species increased with the Ni loading whereas the Ni dispersion decreased with the Ni loading. The Ni metal surface area per gram of catalyst increased with the Ni loading up to 30 wt% and beyond 30 wt%, we observed a decline in Ni metal surface area caused by a drastic increase in the particle size. The number of surface Ni sites followed the same trend. The Ni particle size increased with increase in Ni loading. As Ni loading increased from 5 to 40 wt%, the Ni particle size increased from the 4.8 to 15 nm. Besides, Ni/Si surface composition was obtained from the XPS and presented in Table 2. The surface Ni species were increased from 5 to 30 wt% and decreased beyond that loading. These results are in good agreement with pulse chemisorption where we found maximum number surface Ni species for 30 wt% loading might be due to the high AMSA ($m^2/g_{catalyst}$) and relatively low particle size (8.8 nm).

The surface coverage against the actual Ni content is shown in Fig. 5. The surface coverage of Ni increased with increase in Ni loading up to 30 wt% and thereafter it remained constant. In other words, around 6.5% of surface of the 30 wt% Ni/SBA-15 catalyst was occupied by Ni sites.

SEM image of the reduced 30 wt% Ni/SBA-15 catalyst was illustrated with their corresponding EDAX in Fig. 6. The reduced catalyst has a rod-like shaped morphology by retaining its shape (SBA-15) and Ni particles were well dispersed on the support SBA-15. TEM image of the reduced 30 wt% Ni/SBA-15 catalyst is shown in Fig. 7. Ni particles are found to have good dispersion on the support SBA-15, and the mesoporous support structure can be clearly seen in this image with a honeycomb structure.

TPR experiments were carried out to explore the extent of reducibility of nickel species and the metal–support

Table 2 No. of surface Ni species, dispersion, metal surface area and particle size of Ni/SBA-15 catalysts

Catalyst	*D* (%)	AMSA ($m^2/g_{catalyst}$)	AMSA (m^2/g_{Ni})	Nm (μmol/g)	*D* (nm)	Ni/Si surface composition[a]
5Ni/SBA-15	36.3	12	242	155	2.8	0.16
10Ni/SBA-15	19.0	13	126	162	5.3	0.16
20Ni/SBA-15	14.3	19	95	243	7.1	0.20
30Ni/SBA-15	11.5	20	77	295	8.8	0.36
40Ni/SBA-15	6.7	18	45	228	15.1	0.21

[a]Obtained from XPS

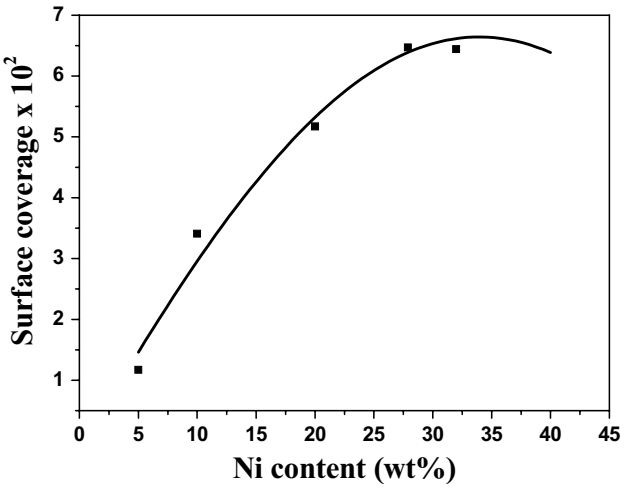

Fig. 5 Relationship between the surface coverage (θ) and actual Ni content

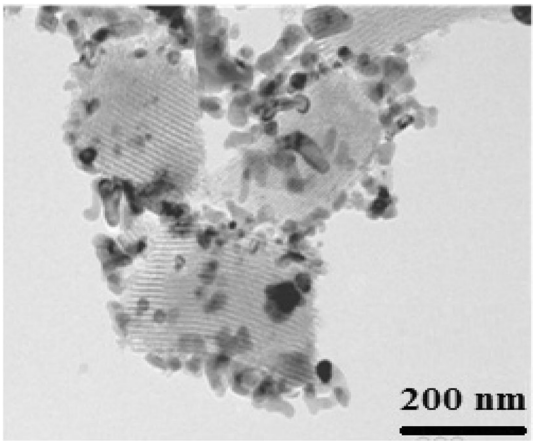

Fig. 7 TEM image and Ni particles distribution of reduced 30Ni/SBA-15 catalyst

interactions [55]. The reduction profiles of the calcined Ni/SBA-15 catalysts are shown in Fig. 8. It is well known that nickel-supported silica catalysts showed different reduction patterns depending on the nature of the interaction between nickel oxide and silica support. Bulk nickel oxide usually gets reduced at around 400 °C [56]. In the present study, the reduction peak observed at a T_{max} of 450 °C can be ascribed to the reduction of Ni^{2+}–Ni^0. The shoulder peak at higher temperature can be assigned to the reduction of nickel oxide that can have strong interaction with the silica [57]. It can inferred from the Figure-8 that as the Ni loading increases, the reduction peak shifted to lower temperature which clearly demonstrates that the presence of bulk Ni is more at higher loadings rather than the dispersed Ni.

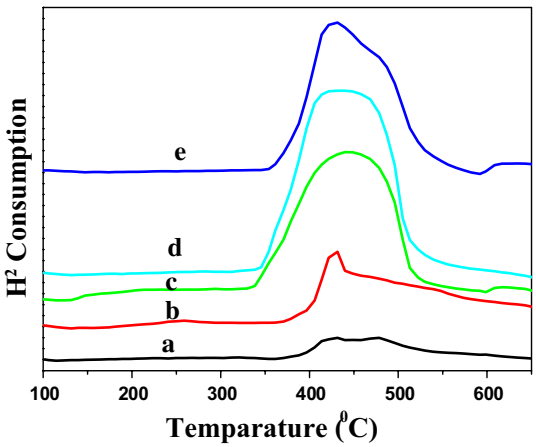

Fig. 8 TPR profiles of **a** 5Ni/SBA-15, **b** 10Ni/SBA-15, **c** 20Ni/SBA-15, **d** 30Ni/SBA-15, **e** 40Ni/SBA-15

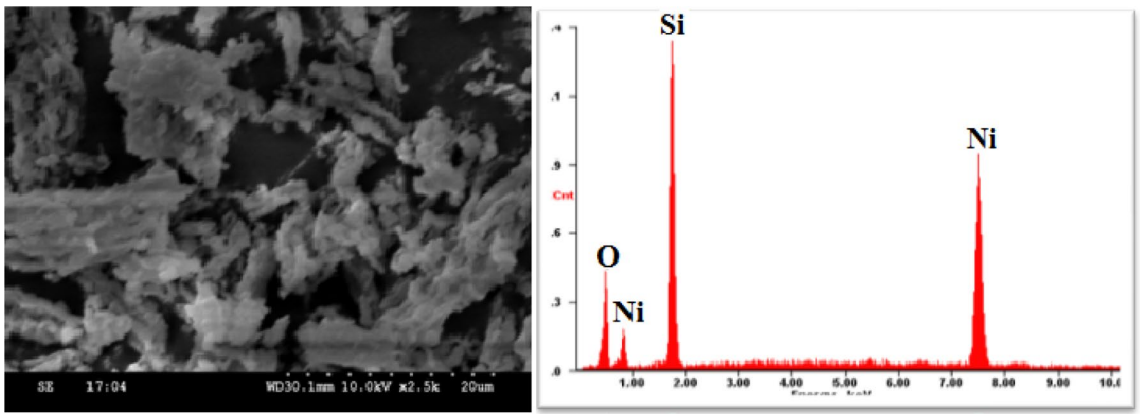

Fig. 6 SEM image and corresponding EDAX patterns of reduced 30Ni/SBA-15 catalyst

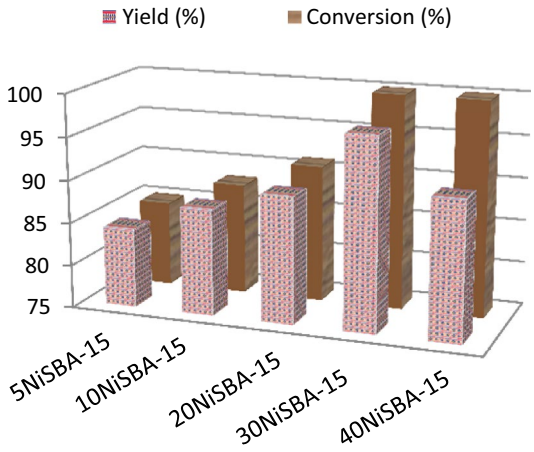

Fig. 9 Effect of Ni loading on the levulinic acid hydro-cyclization over Ni/SBA-15 catalysts. Reaction conditions: Weight of the catalyst = 1 g, temperature = 250 °C, pressure = 1 atm, WHSV = 1 h^{-1}, levulinic acid = 1 ml h^{-1}, carrier gas (H_2) = 1800 ml h^{-1}, H_2/LA molar ratio = 8

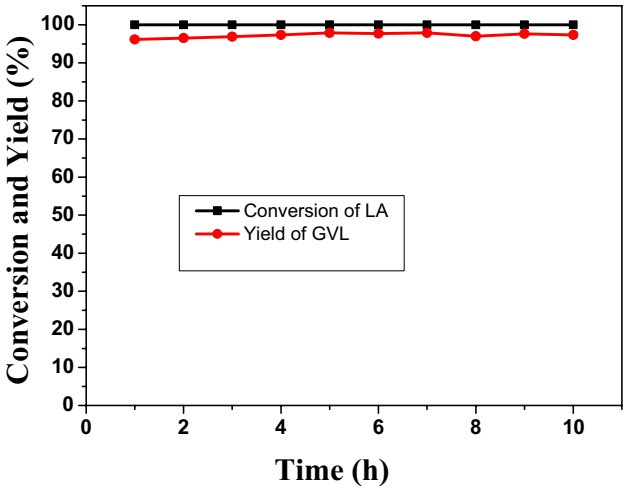

Fig. 10 Influence of time-on-stream over 30Ni/SBA-15 catalysts. Reaction conditions: Weight of the catalyst = 1 g, temperature = 250 °C, WHSV = 1 h^{-1}, pressure = 1 atm, levulinic acid = 1 ml h^{-1}, carrier gas (H_2) = 1800 ml h^{-1}, H_2/LA molar ratio = 8

Catalytic activity

The effects of Ni loading on the hydro-cyclization of LA at optimized conditions are shown in Fig. 9. At 250 °C and 1 atm pressure, 5Ni/SBA-15 showed 85% LA conversion with the selectivity of GVL is 97%. An increase in conversion from 85 to 100%, from 5 to 30 Ni/SBA-15 was witnessed from Fig. 9. The decrease in selectivity to GVL was observed at 40 wt% catalyst due to the formation of by-products such as angelica lactone and valeric acid. The LA conversion increased as the Ni loading increases mainly due to increase in the surface Ni species which is in good agreement with the pulse chemisorption as well as XPS surface composition (both hydrogen uptake and surface composition are in the same order). For the sake of comparison, we evaluated the catalytic performance of 30 wt% Ni/SiO_2 catalyst which showed lower GVL yield (75%) than 30Ni/SBA-15. Despite the fact that the Ni-based catalysts are prominent for cracking no substantial amounts of gaseous products were observed except the reactive gas H_2, which is being left through the hydrogenation of levulinic acid.

Effect of time-on-stream

To assess the stability of the catalyst, time-on-stream analysis was performed over 30Ni/SBA-15 catalyst, and the results are shown in Fig. 10. A stable activity was observed over a period of time for 10 h. The reliable catalytic activity of 30Ni/SBA-15 can be attributed due to the higher number of surface Ni species. Furthermore, both fresh and spent catalysts were evaluated by atomic absorption spectroscopy (AAS) for the content of Ni and no leaching was observed.

In our previous work, the time-on-stream analysis over 30 wt% Ni/HZSM-5 was studied and observed a decline in the activity due to the poisoning by the reaction intermediate (angelica lactone) [34]. In order to avoid the deactivation phenomenon, we adopted various approaches not only coating of carbon on HZSM-5 [58] but also tried various supports [59]. From those results, we realized that the SiO_2 seems to be the best support for this reaction. Afterwards, we performed the hydrogenation of levulinic acid with various architectures of mesoporous silica supported Ni catalysts and noticed an efficient yield of GVL (98%) with full conversion over 2D architectures of mesoporous silica (COK-12) [60]. In this context, we have considered SBA-15 as a support for the levulinic acid hydrogenation to explore the scope of the reaction. The Ni/SBA-15 catalyst exhibited superior selectivity (97%) compared to Ni/HZSM-5 [34] catalyst due to the uniform porous structure of SBA-15.

The relationship of turn over frequency (TOF) with actual Ni content is illustrated in Fig. 11. TOF is defined as the number of LA molecules converted per active Ni site per sec. The number of active Ni sites obtained from the H_2 pulse chemisorptions is shown in Table 2. As evidenced from Fig. 11 that the reaction is structure sensitive up to 10 wt%, above which it is structure insensitive. At low Ni loadings (up to 10%), the Ni particle size is ≤ 5 nm and the intrinsic activity (TOF) is very high in comparison with catalysts containing more than 10 wt% of Ni with particle size ≥ 5 nm. For these catalysts, the TOF values are almost constant.

Moreover, an equimolar formic acid is generated along with the levulinic acid during its production by hydrolysis. Thus, we have evaluated the influence of impurities like

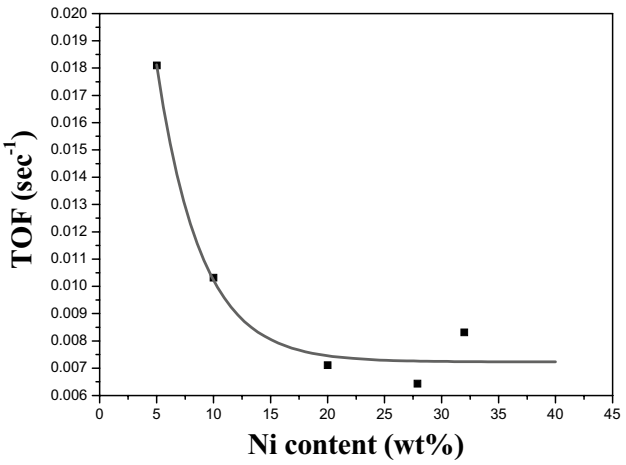

Fig. 11 Relationship between turn over frequency and actual Ni content at 250 °C

formic acid and water on the catalytic performance of the best catalyst, i.e., 30Ni/SBA-15 at an optimized condition. The co-feeding of formic acid with levulinic acid (1:1 molar ratio) in an inert flow (N_2 flow 30 ml min^{-1}) yielded 69% levulinic acid conversion with 45% GVL yield while with the co-feeding of water observed a complete LA conversion with 81% GVL yield. In our earlier publication [61], we have seen a similar observation with nitrobenzene-water mixture over an Ni/SBA-15 catalyst generating ~ 90% yield of aniline which indicated the robustness of SBA-15 as a support. As well, we noticed 22% yield of GVL with 37% levulinic acid conversion over 30 wt% Ni/SiO_2 catalyst (1:1 molar ratio of levulinic acid and formic acid) [58]. This made us to focus on the hydrogenation of levulinic acid with formic acid as the hydrogen source (without external H_2).

Hydrogenation of levulinic acid with formic acid as a H_2 source (without external H_2)

As we have mentioned earlier, this catalytic system is suitable for the hydrogenation of levulinic acid with formic acid as a H_2 source (i.e., without external H_2).Thus, we evaluated the influence of the molar ratio of levulinic acid with formic acid. From the Fig. 12, it can be observed that as the molar ratio (FA/LA) increases from 1:1 to 1:5, the LA conversion also increased from 69 to 100%. Further increase in molar ratio showed a complete LA conversion with decreased selectivity towards the desired product (GVL) owing to the formation of by-products. From these results, one can suggest that the molar ratio 1:5 is optimum for obtaining good yields of GVL.

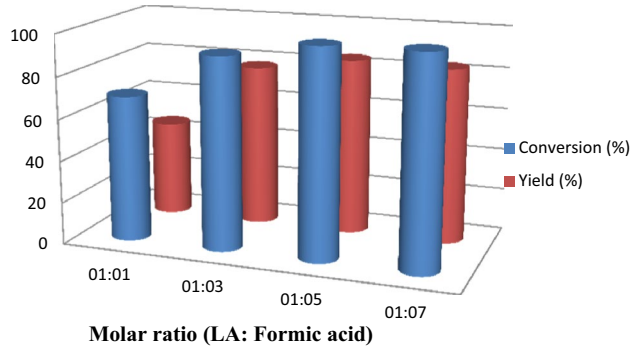

Fig. 12 Influence of molar ratio of levulinic acid and formic acid on the 30Ni/SBA-15 catalyst

Time-on-stream studies of 30Ni/SBA-15 with formic acid as a sole H_2 source (without external H_2)

To gain an insight into the stability of 30Ni/SBA-15 catalyst for the hydrogenation of levulinic acid with formic acid as an H_2 source (without external H_2), we have performed the time-on-stream study for 10 h (Fig. 13). As the time progresses, the decline in activity was noticed. This could be due to the formation of carbon species through the condensation of reaction intermediate on the catalyst surface. To find out the reasons for catalyst deactivation, we performed CHNS analysis and noticed 3 wt% carbon deposition on the spent catalyst. In our previous work, we noticed a drastic decrease in catalytic performance during the time-on-stream on Ni/MgO and Ni/HT due to coking and also water formation during the course of the reaction [62]. Similarly, the continuous decrease of levulinic acid conversion was also observed during the time-on-stream over Ni/SiO_2 catalyst prepared by citric acid assisted method [63]. An advantage of our catalysts prepared on the SBA-15 support implies from its hydrophobicity [61] and a consequent pure coke formation. Further research is devoted to better understanding of the catalyst deactivation phenomenon during the

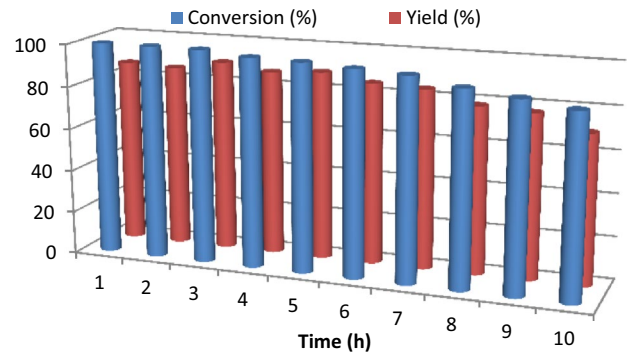

Fig. 13 Time-on-stream study of levulinic acid with formic acid as a sole H_2 source (without external H_2) over 30Ni/SBA-15 catalyst

time-on-stream when the formic acid used as a sole hydrogen source.

Conclusions

Nickel supported on mesoporous silica (SBA-15) was successfully synthesized by means of simple impregnation method. The porous nature of SBA-15 does not alter even after the deposition of high amount of Ni as evidenced by N_2 physisorption, XRD, SEM and TEM images. Ni/SBA-15 is an environmentally benign catalyst for the production of GVL from the hydrogenation of levulinic acid with and without external hydrogen (formic acid as an H_2 source) at atmospheric pressure under additive free conditions. Amongst the series, 30 wt% Ni/SBA-15 showed excellent activity due to the higher number of surface Ni species as suggested by H_2 pulse chemisorption and XPS. Moreover, the catalyst is reliable during the time-on-stream operation of 10 h with external hydrogen flow. These results disclose that Ni-based catalysts are robust and alternative to noble metal catalysts in the hydrogenation of levulinic acid with an external hydrogen source. The decline in catalytic performance during the time-on-stream study in the case of formic acid as an H_2 source is ascribed to the accumulation of carbon species on the catalyst surface.

Acknowledgement The authors are gratefully acknowledges Council of Scientific and Industrial Research, India for the financial support. This research was also financially supported by Basic Science Research Program through the National Research Foundation of Korea (NRF) funded by the Ministry of Education, Republic of Korea (NRF-2016R1A6A1A03013422).

References

1. http://www.mnre.gov.in/schemes/grid-connected/biomass-power cogen/. Accessed 3 Mar 2011
2. Bozell JJ, Moens L, Elliott DC, Wang Y, Neuenscwander GG, Fitzpatrick SW, Bilski RJ, Jarnefeld JL (2000) Production of levulinic acid and use as a platform chemical for derived products. Resour Conserv Recycl 28:227–239. https://doi.org/10.1016/S0921-3449(99)00047-6
3. Gullon P, Romani A, Vila C, Garrote G, Parajo JC (2012) Potential of hydrothermal treatments in lignocellulose biorefineries. Biofuels Bioprod Biorefining 6:219–232
4. Hayes DJ (2009) An examination of biorefining processes, catalysts and challenges. Catal Today 145:138–151
5. He ZS (1999) Extraction of levulinic acid from paper-making black liquor. Chem Ind Eng 2:163–166
6. Dunlop AP, Smith S (1955) US Patent 2676186
7. Manzer LE (2003) US Patent 20030055270
8. Willems GJ, Liska J (1999) EP Patent 933348
9. Shilling WL (1996) US Patent 32355562
10. Crook LR, Jansen BA, Spencer KE, Watson DH (1996) GB Patent 1036694
11. Bart HJ, Reidetschlager J, Schatka K, Lehmann A (1994) Kinetics of esterification of levulinic acid with n-butanol by homogeneous catalysis. Ind Eng Chem Res 33:21–25
12. Varkolu M, Moodley V, Potwana FSW, Jonnalagadda SB, van Zyl WE (2017) Esterification of levulinic acid with ethanol over bio-glycerol derived carbon–sulfonic-acid. Reac Kinet Mech Catal 120:69–80
13. Kopetzki D, Antonietti M (2010) Transfer hydrogenation of levulinic acid under hydrothermal conditions catalyzed by sulfate as a temperature-switchable base. Green Chem 12:656–660
14. Deng L, Zhao Y, Li J, Fu Y, Liao B, Guo QX (2010) Conversion of levulinic acid and formic acid into γ-valerolactone over heterogeneous catalysts. Chemsuschem 3:1172–1175
15. Deng L, Li J, Lai DM, Fu Y, Guo QX (2009) Catalytic conversion of biomass-derived carbohydrates into γ-valerolactone without using an external H_2 supply. Angew Chem Int Ed 48:6529–6532
16. Heeres H, Handana R, Chunai D, Rasrendra CB, Girisuta B, Heeres HJ (2009) Combined dehydration/(transfer)-hydrogenation of C6-sugars (D-glucose and D-fructose) to γ-valerolactone using ruthenium catalysts. Green Chem 11:1247–1255
17. Haan RJ, Lange JP, Petrus L (2007) US Patent 20070208183
18. Mehdi H, Fabios V, Tuba R, Bodor A, Mika LT, Horváth IT (2008) Integration of Homogeneous and heterogeneous catalytic processes for a multi-step conversion of biomass: from sucrose to levulinic acid, γ-valerolactone, 1,4-pentanediol, 2-methyltetrahydrofuran, and alkanes. Top Catal 48:49–54
19. Lange JP, Price R, Ayoub PM, Louis J, Petrus L, Clarke L, Gosselink H (2010) Valeric biofuels: a platform of cellulosic transportation fuels. Angew Chem Int Ed 49:4479–4483
20. Schuette HA, Thomas RW (1930) Normal valerolactone. iii. its preparation by the catalytic reduction of levulinic acid with hydrogen in the presence of platinum oxide. J Am Chem Soc 52:3010–3012
21. Kyrides LP, Groves W, Craver JK (1945) US Patent 2368366
22. Dunlop AP , Madden JW (1957) US Patent 2786852
23. Christian RV Jr, Brown HD, Hixon RM (1947) Derivatives of γ-valerolactone, 1,4-pentanediol and 1,4-Di-(β-cyanoethoxy)-pentane. J Am Chem Soc 69:1961–1963
24. Manzer LE (2003) US Patent 6617464 B2
25. Manzer LE (2004) Catalytic synthesis of α-methylene-γ-valerolactone: a biomass-derived acrylic monomer. Appl Catal A 272:249–256
26. Bourne RA, Stevens JG, Ke J, Poliakoff M (2007) Maximising opportunities in supercritical chemistry: the continuous conversion oflevulinic acid to γ-valerolactone in CO_2. Chem Commun. https://doi.org/10.1039/B708754C
27. Manzer LE, Hutchenson KW (2004) US Patent 2004254384
28. Yan ZP, Lin L, Liu S (2009) Synthesis of γ-valerolactone by hydrogenation of biomass-derived levulinic acid over Ru/C catalyst. Energy Fuels 23:3853–3858
29. Joo F, Beck MT (1975) Formation and catalytic properties of water-soluble phosphine complexes. React Kinet Catal Lett 2:257–263
30. Joo F, Toth Z, Beck MT (1977) Homogeneous hydrogenations in aqueous solutions catalyzed by transition metal phosphine complexes. Inorg Chim Acta 25:L61–L62
31. Osakada K, Ikariya T, Yoshikawa S (1982) Preparation and properties of hydride triphenyl-phosphine ruthenium complexes with

3-formyl (or acyl)propionate [RuH(ocochrchrcor′)(PPh3)3] (R = H, CH3, C2H5; R = H, CH3, C6H5) and with 2-formyl (or acyl) benzoate [RuH(o-OCCOC6H4COR′)(PPh3)3] (R′ = H, CH3). J Organomet Chem 231:79–90
32. Upare PP, Lee J-M, Hwang DW, Halligudi SB, Hwang YK, Chang J-S (2011) Selective hydrogenation of levulinic acid to γ-valerolactone over carbon-supported noble metal catalysts. J Ind Eng Chem 17:287–292
33. Upare PP, Hwang YK, Hwang DW, Lee J-H, Halligudi SB, Hwang J-S, Chang J-S (2011) Direct hydrocyclization of biomass-derived levulinic acid to 2-methyltetrahydrofuran over nanocomposite copper/silica catalysts. Chemsuschem 4:1749–1752
34. Mohan V, Raghavendra C, Pramod CV, Raju BD, Rao KSR (2014) Ni/H-ZSM-5 as a promising catalyst for vapour phase hydrogenation of levulinic acid at atmospheric pressure. RSC Adv 4:9660–9668
35. Dodds DR, Gross RA (2007) Chemicals from Biomass. Science 318:1250–1251
36. Corma A, Iborra S, Velty A (2007) Chemical routes for the transformation of biomass into chemicals. Chem Rev 107:2411–2502
37. Jessop PG (2011) Searching for green solvents. Green Chem 13:1391–1398
38. Horváth IT, Mehdi H, Fábos V, Boda L, Mika LT (2008) γ-Valerolactone—a sustainable liquid for energy and carbon-based chemicals. Green Chem 10:238–242
39. Bond JQ, Alonso DM, Wang D, West RM, Dumesic JA (2010) Integrated catalytic conversion of γ-valerolactone to liquid alkenes for transportation fuels. Science 327:1110–1144
40. Kim SW, Son SU, Lee SL, Hyeon T, Chung YK (2000) Cobalt on mesoporous silica: the first heterogeneous pauson−khand catalyst. J Am Chem Soc 122:1550–1551
41. Iglesia E, Boudart M (1983) Decomposition of formic acid on copper, nickel, and copper-nickel alloys: I. preparation and characterization of catalysts. J Catal 84:204–213
42. Hengne AM, Malawadkar AV, Biradar NS, Rode CV (2014) Surface synergism of an Ag–Ni/ZrO_2 nanocomposite for the catalytic transfer hydrogenation of bio-derived platform molecules. RSC Adv 4:9730–9736
43. Bulushev DA, Ross JRH (2011) Vapour phase hydrogenation of olefins by formic acid over a Pd/C catalyst. Catal Today 163:42–46
44. Yamamoto K, Sunagawa Y, Takaha hi H, Muramatsu A (2005) Metallic Ni nanoparticles confined in hexagonally ordered mesoporous silica material. Chem Commun 348–350.
45. Chary KVR, Srikanth CS (2009) Selective hydrogenation of nitrobenzene to aniline over Ru/SBA-15 catalysts. Catal Lett 128:164–170
46. Li H, Xu Y, Yang H, Zhang F, Li H (2009) Ni-B amorphous alloy deposited on an aminopropyl and methyl co-functionalized SBA-15 as a highly active catalyst for chloronitrobenzene hydrogenation. J Mol Catal A: Chem 307:105–114
47. Zhao D, Feng J, Huo Q, Melosh N, Fredrickson GH, Chmelka BF, Stucky GD (1998) Triblock copolymer syntheses of mesoporous silica with periodic 50 to 300 angstrom pores. Science 279:548–552
48. Gregg SJ, Sing KSW (1982) Adsorption, surface area and porosity, 2nd edn. Acadamic Press, New York
49. Zhao DY, Huo Q, Feng J, Chmelka BF, Stucky GD (1998) Nonionic triblock and star diblock copolymer and oligomeric surfactant syntheses of highly ordered, hydrothermally stable, mesoporous silica structures. J Am Chem Soc 120:6024–6036
50. Lihui Z, Jun HU, Songhai XIE, Honglai LIU (2007) Dispersion of active Au nanoparticles on mesoporous SBA-15 materials. Chin J Chem Eng 15(4):507–511. https://doi.org/10.1016/S1004-9541(07)60116-5
51. Rioux RM, Song H, Hoefelmeyer JD, Somorjai GA (2005) High-Surface-Area catalyst design: synthesis, characterization, and reaction studies of platinum nanoparticles in mesoporous SBA-15 silica. J Phys Chem B 109:2192–2202
52. Wang X, Wang P, Dong Z, Dong Z, Ma Z, Jiang J, Li R, Ma J (2010) Highly sensitive fluorescence probe based on functional SBA-15 for selective detection of Hg^{2+}. Nanoscale Res Lett 5:1468–1473
53. Ladavos AK, Katsoulidis AP, Iosifidis A, Triantafyllidis KS, Pinnavaia TJ (2012) The BET equation, the inflection points of N2 adsorption isotherms and the estimation of specific surface area of porous solids. Micro Meso Mater 151:126–133
54. Zhang F, Yan Y, Yang H, Meng Y, Yu C, Tu B, Zhao D (2005) Understanding effect of wall structure on the hydrothermal stability of mesostructured silica SBA-15. J Phys Chem B 109:8723–8732
55. Mile B, Steriling D, Zammitt MA (1990) TPR studies of the effects of preparation conditions on supported nickel catalysts. J Mol Catal 62:179–198
56. Wu T, Yan Q, Wan H (2005) Partial oxidation of methane to hydrogen and carbon monoxide over a Ni/TiO_2 catalyst. J Mol Catal A: Chem 226:41–48
57. Diskin AM, Cunningham RH, Ormerod RM (1998) The oxidative chemistry of methane over supported nickel catalysts. Catal Today 46(2/3):147–155
58. Mohan V, Raju BD, Rao KSR (2015) Vapour phase hydrogenation of levulinic acid over carbon coated HZSM-5 supported Ni catalysts. J Catal Catal 2(2):33–38
59. Mohan V, Venkateshwarlu V, Pramod CV, Raju BD, Rao KSR (2014) Vapour phase hydrocyclisation of levulinic acid to γ-valerolactone over supported Ni catalysts. Catal Sci Technol 4:1253–1259
60. Varkolu M, Velpula V, Ganji S, Burri DR, Kamaraju SRR (2015) Ni nanoparticles supported on mesoporous silica (2D, 3D) architectures: highly efficient catalysts for the hydrocyclization of biomassderived levulinic acid. RSC Adv 5:57201–57210
61. Mohan V, Pramod CV, Suresh M, Hari KHP, Raju BD, Rao KSR (2012) Advantage of Ni/SBA-15 catalyst over Ni/MgO catalyst in terms of catalyst stability due to release of water during nitrobenzene hydrogenation to aniline. Catal Commun 18:89–92
62. Varkolu M, Velpula V, Burri DR, Kamaraju SRR (2016) Gas phase hydrogenation of levulinic acid to γ-valerolactone over supported Ni catalysts with formic acid as hydrogen source. New J Chem 40:3261–3267
63. Varkolu M, Burri DR, Kamaraju SRR, Jonnalagadda SB, van Zyl WE (2017) Hydrogenation of levulinic acid using formic acid as a hydrogen source over Ni/SiO_2 catalysts. Chem Eng Technol 40:719–726